# Rupture Status Discrimination in Intracranial Aneurysms using the Centroid-Radii Model

Alexandra Lauric, Eric L. Miller, *Senior Member, IEEE,*, Merih I. Baharoglu, and Adel M. Malek

***Abstract*—Intracranial aneurysms are localized, abnormal arterial dilatations with a variable risk of rupture, leading to medical conditions associated with high morbidity and mortality. Predicting their risk of rupture, especially for incidental asymptomatic aneurysms, is a challenging task. The size of the aneurysm sac is traditionally used to assess the risk, but shape analysis has emerged as a promising differentiator of rupture likelihood. The centroid-radii model (CRM) is introduced here to describe both the size and the shape of the aneurysms, and determine rupture status. The entropy of CRM is proposed as an aneurysm descriptor which is easy to compute, robust to noise and segmentation, and accurate in rupture status discrimination. Analysis is performed on 154 patient-derived saccular aneurysms. The aneurysms are further classified as sidewall and bifurcation, and the shape analysis is performed separately on the two subtypes. Using the entropy of CRM resulted in 80.3% and 70.5% classification accuracy of status rupture in sidewall and bifurcation aneurysms, respectively. When compared to the accuracy of some commonly used size and shape indexes, the entropy of CRM proved to be a more accurate single index associated with rupture in intracranial aneurysms, for both sidewall and bifurcation subtypes.**

***Index Terms*—Brain aneurysms, shape analysis, 3D geometry, 3D morphology, centroid-radii model, entropy.**

## I. Introduction

An intracranial cerebral aneurysm is a localized pathological dilatation of a brain vessel. It is reported that up to 2% of the general population harbors aneurysms [1], although some autopsy and angiography studies indicate this number could be as high as 6% [2]. The majority of cerebral aneurysms are asymptomatic and remain undetected. However, recent advances in imaging technologies and the increasing use of computed tomography (CT) and magnetic resonance (MR) imaging in outpatient settings, have led to an increased detection of incidental, asymptomatic unruptured intracranial aneurysms (UIA) [3]. While, with rare exceptions, the recommendation is for all unruptured symptomatic aneurysms to be treated, the management of asymptomatic UIA remains controversial [4], [5]. On one hand, should the aneurysm rupture, the initial bleed carries high mortality and morbidity rates and despite improvements in patient management, the incidence of subarachnoid hemorrhage (SAH) has not declined over time [2]. On the other hand, recent studies estimate the annual rupture rate of a prospectively monitored selected patient population at only 0.1-0.2% [6], in contrast with earlier data which reported an annual rupture rate of 1-2% [2]. Since preventive treatment carries risks of complications which increase with age [6], the decision to intervene and treat UIA needs to be balanced against the risk of rupture. To this end, the International Study of Unruptured Intracranial Aneurysms (ISUIA) released the conclusions of two studies in 1998 and 2003 with the goal of defining an optimal treatment strategy of UIA [6], [7]. The size and location of the aneurysms were concluded to play important roles in predicting rupture risk and a threshold of 7 mm diameter was proposed. Under the influence of ISUIA studies, predicting rupture in UIA has focused mainly on the size of the aneurysm, and other size related indexes such as aspect ratio (AR) and height-width (H/W) ratio [8].

Cerebral aneurysms present in various shapes and three-dimensional sizes and, like size, shape is likely to have an impact on the rupture risk [8]–[10]. With advances in medical imaging, modalities such as 3D rotational angiography (3D-RA), computed tomography angiography (CTA) and magnetic resonance angiography (MRA) can capture the complexity of the volumetric shape and offer the possibility to analyze aneurysms in a 3D environment. Still, the morphological characterization of cerebral aneurysms remains an open research area. Ma *et al.* [11] and Raghavan *et al.* [9] proposed some of the first parameters to describe the 3D geometry of cerebral aneurysms and introduced global descriptors such as undulation, non-sphericity and ellipticity indexes. These parameters were further discussed in [8], [10]. More complex shape analysis was performed in [12] using Fourier analysis and in [13] using geometric and Zernike moments.

The purpose of this current work is to further investigate the potential of 3D shape characterization of intracranial aneurysms in rupture status analysis. Because of the nature of the application, the goal is to propose descriptors that are not only robust and effective in differentiating rupture status, but also intuitive to the medical community which is the ultimate user of such a tool. To this end, this study introduces an automated methodology to characterize the 3D shape of intracranial aneurysms based on the centroid-radii model (CRM) [14], [15]. CRM provides a compact representation of a shape and it is currently used in pattern recognition and shape retrieval applications [16], [17]. Under the model, distances between the centroid and the boundary of the aneurysm are computed in all directions. The resulting distribution of unnormalized distances describes both the size and the shape of the aneurysms. CRM, as used here, is

A. Lauric is with the Department of Neurosurgery, Tufts Medical Center, Boston MA 02111 USA (e-mail alauri02@eecs.tufts.edu).

E. Miller is with the Department of Electrical and Computer Engineering, Tufts University, Medford MA 02155 USA (e-mail elmiller@ece.tufts.edu).

M. I. Baharoglu and A. M. Malek are with the Department of Neurosurgery, Tufts Medical Center, Boston MA 02111 USA (e-mail amalek@tuftsmedicalcenter.org).

translation and rotation invariant. When the distances are normalized by division with the largest distance, CRM is scale invariant and the resulting distribution describes only the shape of the aneurysms. The entropy of both normalized and unnormalized distance distributions are introduced as powerful indexes to describe rupture status.

The morphological analysis was performed on a database of 154 saccular aneurysms (73 ruptured) derived from 3D rotational angiography imaging studies. Similar to recent morphological studies [8], [9], [11]–[13] the rupture status classification is performed on a dataset of aneurysms which were labeled as being ruptured or not at the time of detection by the treating physicians. The rupture status classification results using CRM entropy were compared with the performance of six established 2D (size, AR, HW) and 3D (ellipticity, undulation, non-sphericity) indexes.

The paper is structured as follows: details about some commonly used size and shape indexes, as well as the proposed centroid-radii model are presented in Section II. Sections III and IV describe our data and methodology. Results and robustness analysis are detailed in Section V. Discussion, conclusions and directions for future work are presented in Section VI.

## II. Related Work

### A. Established Size and Shape Indexes

The performance of the shape index proposed in this study is compared against the performance of six existing size and shape indexes which are described in this section.

*1) Size Indexes:* The largest diameter of the aneurysm ($D_{max}$) is the most commonly used index to clinically asses rupture risk. Two other potentially useful indexes, especially for small aneurysms which might be missed by the largest diameter measure, are aspect ratio (AR) (aneurysm height/neck width) [18] and height-width (H/W) (aneurysm height/largest diameter) [11] (Fig. 1).

For this work the size indexes described above were measured manually in a blinded fashion by an experienced clinical operator. Size measurements were validated by a second clinical operator (interclass correlation coefficient 0.92). All measurements were performed on the 3D model of each aneurysm using Amira, a 3D visualization and modeling system (Visage Imaging, San Diego CA).

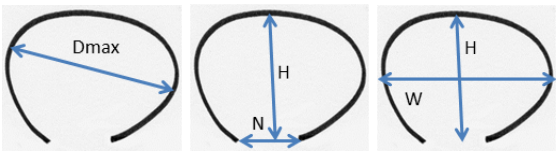


Fig. 1. Existing size indexes (a) Largest diameter size. (b) Aspect ratio is defined as height $H$ divided by neck diameter $N$ (c) Height-width index is defined as the height $H$ divided by width $W$.

*2) Shape Indexes:* The non-sphericity index (NSI) [9] measures how closely the shape of the aneurysm resembles an ellipsoid. The index is defined as $NSI = 1 - (18\pi)^{\frac{1}{3}} \frac{V^{\frac{2}{3}}}{S}$, where $V$ is the aneurysm volume and $S$ is the aneurysm surface. The NSI varies from 0 to 1, being 0 for a hemisphere and increasing with deviation from a spherical shape due to ellipticity or undulations in the surface. The ellipticity index (EI) [9] measures how close the shape of the aneurysm is to an ellipsoid. The index is defined as $EI = 1 - (18\pi)^{\frac{1}{3}} \frac{V_{ch}{}^{\frac{2}{3}}}{S_{ch}}$, where $V_{ch}$ is the volume of the aneurysm convex hull and $S_{ch}$ is the surface of the aneurysm convex hull. EI varies from 0 to 1, being 0 for a sphere and increasing with ellipticity. The undulation index (UI) [9] describes irregularities on the surface of the aneurysm. The index is defined as $UI = 1 - \frac{V}{V_{ch}}$, where $V_{ch}$ is the volume of the aneurysm convex hull and $V$ is the aneurysm volume. The UI varies from 0 to 1, being 0 for convex aneurysm and increasing with the presence of surface irregularities and lobulations. The EI, UI and NSI indexes are some of the first 3D shape descriptors to be associated with aneurysm rupture risk and to be included in relevant clinical research studies [8]–[10].

For this work, the shape indexes described above were computed automatically from the aneurysm models, using in-house MATLAB (MathWorks, Natick MA) routines.

### B. The Centroid-Radii Model

The centroid-radii model for shape representation was proposed by [14] and refined by [15]. The centroid-radii model represents an object by its star-shaped envelope with respect to the centroid (Fig. 2). An object is said to be star-shaped if there exists a point C interior to the shape, in this case the centroid, such that for every point P on the surface of the object, the line segment PC lies entirely within the object. In other words, every point on the surface of the object is visible from point C. The original work describes 2D shapes and the angle between consecutive radii is fixed. For 3D objects, the model uses distances from the centroid to the discretized surface of an object (meshes, point clouds). Because the distances are computed from the centroid, the model is translation invariant. The model can be normalized and made scale invariant by dividing all distances by the largest radius. When used to compare two similar objects, the model captures the salient features of their shapes, while discarding small shape variations. The centroid-radii model provides a compact representation of a shape, usually in a multidimensional format such as histograms and distance arrays. The model is used in pattern recognition and shape retrieval applications [16], [17].

CRM is similar to the spherical extent function, which is a ray-based 3D descriptor used in database retrieval applications [19], [20]. Similarly to CRM, the spherical extent function captures the closest intersection points between rays emanating from the center of mass and the surface of the object.

Figure 2 shows how the star-shaped envelope of a 3D shape can differ from the original model. This is the only aneurysm in the dataset which differs from its star-shape envelope with more than 5% (92% overlap between original surface and its envelope). In our experiments, 93% of the aneurysms are star-shaped with respect to their centroids. For the remaining 7%, on average, the star-shaped envelope overlaps the actual

TABLE I
DETAILS ABOUT ANEURYSM DISTRIBUTION BASED ON LOCATION, RELATION WITH THE PARENT VESSEL (BF VS. SW) AND RUPTURE STATUS (RUPTURED (Y) VS. UNRUPTURED (N).

| Location | N | SW | | BF | |
|---|---|---|---|---|---|
| | | n | y | n | y |
| Anterior Communicating | 41 | | | 7 | 34 |
| Posterior Communicating | 33 | 13 | 11 | 5 | 4 |
| Middle Cerebral | 25 | | | 23 | 2 |
| Internal Carotid | 18 | 14 | 4 | | |
| Internal Carotid Artery Bifurcation | 10 | | | 9 | 1 |
| Ophthalmic Artery | 8 | 5 | 3 | | |
| Basilar | 8 | | | 2 | 6 |
| Anterior Choroidal Artery | 5 | 2 | 3 | | |
| Vertebral | 3 | 1 | 2 | | |
| Posterior Inferior Cerebellar Artery | 2 | | | | 2 |
| Cuperior Cerebellar Artery | 1 | | | | 1 |

aneurysm on more than 98% of the surface. This indicates that using CRM does not result in a loss of shape information.

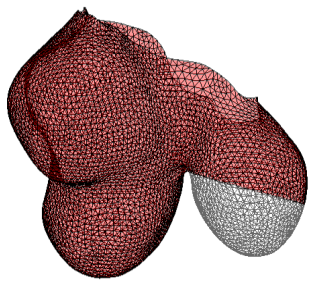

Fig. 2. The star-shaped envelope (in red) can differ from the original model (in gray). The shape represents a ruptured sidewall aneurysm. There is 92% surface overlap between the original shape and its envelope.

## III. CLINICAL DATA

The clinical database consists of 154 distinct cerebral aneurysms from 137 consecutive patient-derived 3D rotational angiography (3D-RA) imaging studies. Data (collected between 2001-2005) were acquired using a biplane flat-detector digital subtraction angiography system. The size of each 3D-RA volume is 128x128x128 voxels with 0.48 mm isotropic spacing. Approval for the collection and review of data was obtained from the Institutional Review Board.

Aneurysms were labeled as ruptured (73) and unruptured (81) based on presentation at the time of the initial evaluation, by the treating physicians (Table I). The aneurysms were further classified as sidewall (SW) (dilation of the artery in one direction perpendicular to the vessel axis - 58 aneurysms) and bifurcation (BF) (dilation at the bifurcation of arteries - 96 aneurysms). Fusiform aneurysms are not considered in this study given how different their pathology and morphology are from that of saccular aneurysms [21]. The average largest diameter of the aneurysms in the database is 6.92$\pm$3.14 mm.

## IV. METHOD

### A. Method Overview

The following methodology is proposed to differentiate aneurysm rupture status based on the centroid-radii model. Using a 3D visualization and modeling system, the cerebral vasculature is segmented from the 3D-RA volume and a 3D model is created for each aneurysm by isolating the aneurysm sac from its adjacent parent vessels. The model is represented as a triangular mesh and saved in STL (stereolithography) file format, which describe the surface geometry of a 3D object as a collection of vertices and associated faces. The resulting STL files represent the input to MATLAB routines, which are used to apply the centroid-radii model, perform histogram smoothing and compute histogram statistics. More specifically, centroid-radii distances are computed along the surface of the model. Normalized and unnormalized distances are stored in two distance histograms. Histogram smoothing is performed using kernel estimators. The entropy of each distance distribution is used as a classification feature for rupture status discrimination. Details are presented below.

### B. Segmentation and Isolation of Aneurysms

Figure 3 shows the steps performed on the original 3D-RA volume (Fig. 3(a)), in order to obtain the aneurysmal sac isolated from the surrounding vessels (Fig. 3(f)). Image processing operations, including segmentation, are performed using Amira, a 3D visualization and modeling system (Visage Imaging, San Diego CA). The original 3D-RA data did not require any smoothing operations. Similar to Bescos et al. [22], edge-detection was used to guide the segmentation, with the difference that the Sobel filter was preferred to the Canny edge-detection. Sobel edge detection was chosen because it is fast and does not require any input parameters. First, the Sobel edge detection filter is applied to the original volume (Fig. 3(b)). Second, an initial isosurface is automatically created using a default threshold value. The isosurface is refined by visual inspection such that the final surface sits within the Sobel edges ((Fig. 3(c)). It has been found that, using the Sobel filter in guiding the segmentation process, results in a very narrow range of acceptable threshold values. The segmented surface is automatically generated and represented as a triangular mesh (Fig. 3(d)). A cutting plane, tangent to the surface of the vessels (Fig. 3(e)), is identified visually at the location where the aneurismal sac originates from the parent vessels [10], by taking into account the local geometry of the vasculature. The aneurysm model is represented as a triangulated mesh and store in an STL file.

### C. Centroid-Radii Distances Computation

Centroid-radii distance analysis is performed in MATLAB on each 3D STL model. For each vertex in the mesh, a ray originating from the centroid is shot in the direction of that vertex. The first intersection of the ray with the surface of the aneurysm is recorded. The number of ray-triangle intersections is reduced by use of octree space partitioning [23]. Each aneurysm is described by two sets of distances: a set of unnormalized distances and a set of normalized distances obtained by dividing each unnormalized distance by the maximum unnormalized distance. The algorithm for CRM distance computation is completely automated.

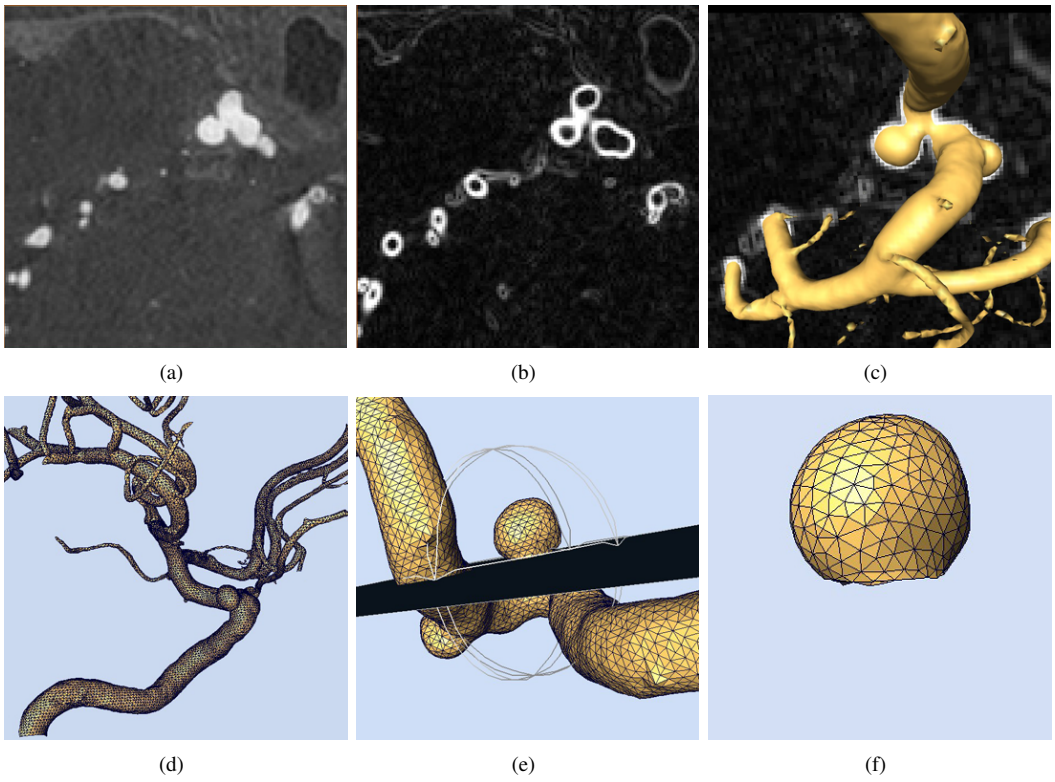


Fig. 3. Segmentation and isolation of aneurysms. (a) Original 3D-RA data (b) Sobel edge detection filter (c) Threshold value based on Sobel filter (d) Surface is represented as a triangular mesh (e) Cutting plane is tangent to the aneurysm surface (f) The aneurysm sac is completely separated from vessels.

### D. Histogram Statistics

Distance values along the surface of each aneurysm are represented using a frequency histogram. The value of each bin is divided by the total number of samples, and the area under the counting bins adds to one. The histogram is a non-smooth estimator of the underlying density function showing discontinuities at its ends and at bins with zero value. To avoid these shortcomings, histogram smoothing is performed using Nadaraya-Watson estimator (Eq. 1) with Gaussian kernels [24] whose bandwidth (Eq. 2) is selected using the method of Bowman *et al.* [25]

$$\hat{m_h}(x) = \sum_{i=1}^{n} \frac{Y_i K_h(x - X_i)}{\sum_{j=1}^{n} K_h(x - X_j)} \quad (1)$$

$$h = (\frac{4}{3n})^{1/5}\sigma \quad (2)$$

where $K_h$ is the smoothing kernel with bandwidth h, $X_i$ are distance samples with associated $Y_i$ frequencies. Bandwidth $h$ is computed as a function of the standard deviation of the distribution $\sigma$. The entropy is computed from the smoothed histogram and, for a continuous random variable $x$, with density $p(x)$, is a measure of the uncertainty associated with that variable. It is defined as

$$h(x) = -\int_x p(x) \log p(x) dx. \quad (3)$$

The entropy does not depend on the values of $x$, but only on the probabilities that $x$ will occur [26]. Intuitively, the entropy is a measure of how well organized the data ~~is~~ and how predictable is a random sample variable. Uniform probability distributions, which show maximum uncertainty, have maximum entropy.

### E. Classification

The classification problem solved here involves two classes (ruptured vs. unruptured) and 154 samples described each by two features: the entropy of the unnormalized distance distribution ($CR_h$) and the entropy of the normalized distance distribution ($CR_{hnorm}$). The method used is logistic regression with 10-fold cross-validation [27]. The classification is repeated 10 times with 10 different random seeds. This results in 100 different data splittings. The average performance is reported.

## V. Results

### A. Rupture Status Prediction

In this study, the performance of an index in rupture status discrimination is quantified using two measures: the classification accuracy (percentage of correctly labeled samples) and the area under the receiver operating characteristic (ROC) curve. The ROC curve is a graphical representation of the performance of a binary classifier as its discrimination threshold is varied. The sensitivity of the method (true positives rate) is plotted vs. the specificity of the method (false positives rate). The area under the ROC curve (AUC) represents the trade-off between true positive and false positive and takes values

between 0 and 1. A perfect classification method has 100% sensitivity (all true positives are identified), 100% specificity (no false positives) and an AUC of 1.

First, the classification is performed using each of the six size and shape indexes presented in Section II-A. Table II shows the rupture status classification performance for the whole set of 154 aneurysms (SW+BF) and for subsets of SW and BF aneurysms. All indexes perform better on SW than on BF aneurysms. For SW aneurysms, NSI has the best classification accuracy (77.1%), followed by $D_{max}$, the largest diameter index (70.6%). For BF aneurysms, UI has the best classification accuracy (66.8%), followed by H/W (63.7%).

Second, classification is performed using the entropy of the CRM model. Table III summarizes the main results of this study. The two indexes evaluated are the entropy of the normalized distance distribution ($CR_{hnorm}$) and the entropy of the unnormalized distance distribution ($CR_h$). Classification is performed on the three subsets: 154 SW+BF, 58 SW and 96 BF. For the SW aneurysms, $CR_h$ works best and results in 80.3% accuracy, with an AUC of 0.85. For the BF aneurysms, $CR_{hnorm}$ works best and results in 70.5% accuracy, with an AUC of 0.75. The result suggest that both shape and size are relevant for rupture in SW aneurysms, whereas shape is more relevant than size for rupture risk in BF aneurysms. For the SW+BF group, $CR_h$ works best (67.2% accuracy), a result of the SW vs. BF ratio in our dataset.

Figure 4 shows the ROC curves corresponding to the performance of $D_{max}$, NSI, $CR_h$ and $CR_{hnorm}$ indexes, both for the SW+BF group (Fig. 4(a)), and also within SW (Fig. 4(b)) and BF (Fig. 4(c)) subgroups. The graphics show that $CR_h$ is a good performer in the SW group, while $CR_{hnorm}$ performs best in the BF group. Given the difference in performance between the SW and BF groups for all indexes studied here, we also use ROC curves to show these differences for $D_{max}$ (Fig. 4(d)), $CR_h$ (Fig. 4(e)) and $CR_{hnorm}$ (Fig. 4(f)) indexes. Indeed, the graphics show that $D_{max}$ has a poor performance in the BF group compared to SW group. As expected, $CR_h$ performs best in the SW group. In contrast with all other indexes studied, $CR_{hnorm}$ has a very balanced performance, as its accuracy and AUC values are very similar for all three aneurysm groups.

The means and standard deviations of the proposed entropy indexes are calculated separately for the ruptured and unruptured subsets. A two-tailed independent Student's test was performed to assess the statistical significance of the observed differences between the means of ruptured and unruptured aneurysms as indicated by the p-values (Table IV). A p-value smaller than 0.05 is considered to be statistically significant. The results indicate that statistics for both normalized and unnormalized indexes perform well at distinguishing between ruptured and unruptured subsets.

The differences between ruptured and unruptured aneurysms as captured by the CRM are apparent in Fig. 5 and 6 which show analysis results on SW and BF aneurysms respectively. In the figures, centroid-radii distance values are shown along the surface of ruptured and unruptured aneurysms, and the corresponding histograms. SW aneurysms are represented in Fig. 5 using unnormalized distances, whereas BF aneurysms

TABLE II
PERFORMANCE OF RUPTURE PREDICTION FOR SIZE AND SHAPE INDEXES, AS QUANTIFIED BY ACCURACY AND AUC VALUES.

| Type | Feature | Accuracy % | AUC |
|---|---|---|---|
| SW+BF | NSI | 66.0 | 0.73 |
| SW+BF | UI | 63.6 | 0.70 |
| SW+BF | EI | 62.2 | 0.67 |
| SW+BF | H/W | 60.4 | 0.68 |
| SW+BF | AR | 58.8 | 0.67 |
| SW+BF | Dmax | 57.5 | 0.59 |
| SW | NSI | 77.1 | 0.77 |
| SW | Dmax | 70.6 | 0.75 |
| SW | AR | 69.2 | 0.72 |
| SW | UI | 68.6 | 0.74 |
| SW | H/W | 67.2 | 0.76 |
| SW | EI | 61.6 | 0.66 |
| BF | UI | 66.8 | 0.71 |
| BF | H/W | 63.7 | 0.63 |
| BF | EI | 61.8 | 0.68 |
| BF | AR | 61.0 | 0.65 |
| BF | NSI | 60.5 | 0.68 |
| BF | Dmax | 48.7 | 0.43 |

TABLE III
PERFORMANCE OF RUPTURE PREDICTION FOR CRM ENTROPY, AS QUANTIFIED BY ACCURACY AND AUC VALUES.

| Type | Feature | Accuracy % | AUC |
|---|---|---|---|
| SW+BF | $CR_h$ | 63.8 | 0.68 |
| SW+BF | $CR_{hnorm}$ | 67.2 | 0.73 |
| SW | $CR_h$ | 80.3 | 0.85 |
| SW | $CR_{hnorm}$ | 64.3 | 0.75 |
| BF | $CR_h$ | 56.1 | 0.59 |
| BF | $CR_{hnorm}$ | 70.5 | 0.75 |

are represented in Fig. 6 using normalized distances. The approximating probability distribution of CRM is shown in red. Unruptured aneurysms tend to be smaller and have a more spherical shape [10], resulting here in sharp distance distributions and low entropy. Ruptured aneurysms, which tend to have more irregular, non-spherical shapes [10], have here a more spread out distance distribution, associated with higher entropy. As a consequence, ruptured aneurysms have significantly higher entropy of the centroid-radii distance distribution, when compared to unruptured aneurysms (Table IV).

Note that, despite its irregular, non-convex shape, the ruptured BF aneurysm shown in Fig. 6(b) is completely star-shaped with respect to its centroid. Its rupture status was correctly classified by the method. At the same time, the ruptured SW aneurysm shown in Fig. 2 was also correctly classified by the method.

### *B. Sensitivity to Segmentation*

To determine the sensitivity of the method to segmentation, a second segmentation based on level sets [28] is employed on the original 3D-RA dataset of 58 SW aneurysms, using a different visualization system (ITK-SNAP31). The analysis involves four classification cases: two in which the training and the testing sets are segmented using the same method, and two in which the training and the testing sets are segmented using different methods (Table V). The entropy of the CRM

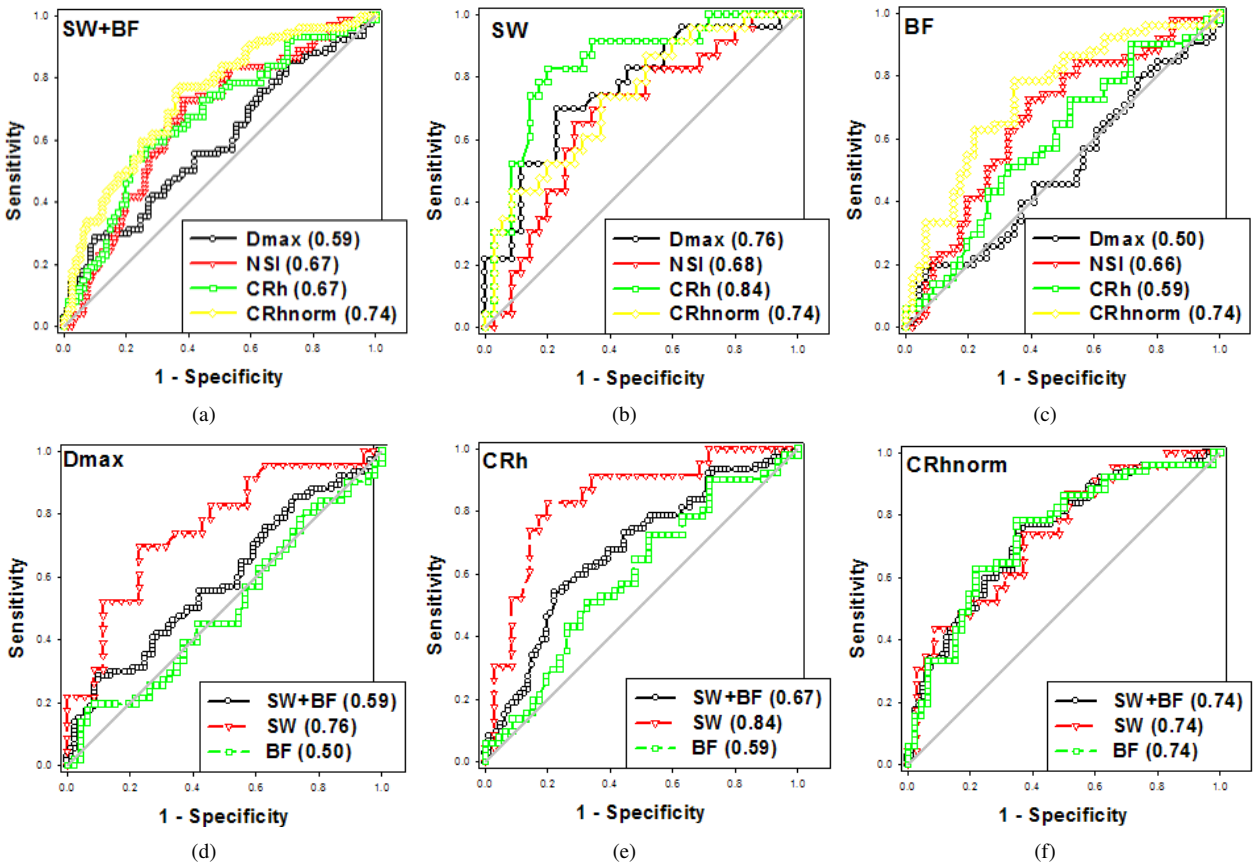


Fig. 4. ROC analysis. AUC values shown in parenthesis. Comparison between $D_{max}$, NSI, $CR_h$ and $CR_{hnorm}$ for the (a) SW+BF, (b) SW and (c) BF groups. Comparison between SW+BF, SW and BF groups using the (d) $D_{max}$, (e) $CR_h$ and (f) $CR_{hnorm}$ indexes.

TABLE IV
POPULATION VARIATION (MEAN, STANDARD DEVIATION) WITHIN THE CRM INDEXES.

| Type | Feature | Unuptured | Ruptured | p-value |
|---|---|---|---|---|
| SW+BF | $CR_h$ | $0.84 \pm 0.28$ | $1.02 \pm 0.30$ | 0.0002 |
| SW+BF | $CR_{hnorm}$ | $0.060 \pm 0.006$ | $0.066 \pm 0.006$ | $< 0.0001$ |
| SW | $CR_h$ | $0.81 \pm 0.26$ | $1.16 \pm 0.25$ | $< 0.0001$ |
| SW | $CR_{hnorm}$ | $0.059 \pm 0.007$ | $0.065 \pm 0.008$ | 0.0003 |
| BF | $CR_h$ | $0.87 \pm 0.29$ | $0.97 \pm 0.30$ | 0.1280 |
| BF | $CR_{hnorm}$ | $0.061 \pm 0.006$ | $0.066 \pm 0.006$ | $< 0.0001$ |

TABLE V
SENSITIVITY OF THE CRM-BASED CLASSIFICATION TO SEGMENTATION.

| Train set | Test set | Feature | Accuracy % | AUC |
|---|---|---|---|---|
| Threshold | Threshold | $CR_h$ | 80.3 | 0.85 |
| Threshold | Level Sets | $CR_h$ | 79.7 | 0.81 |
| Level Sets | Level Sets | $CR_h$ | 81.7 | 0.86 |
| Level Sets | Threshold | $CR_h$ | 80.7 | 0.83 |

distribution is very robust to segmentation and similar results are obtained regardless of the segmentation method used on training and testing data ($\approx 80\%$). Distances from centroid to the surface of the aneurysms are less sensitive to the small variation between segmentation methods and are more robust to different degrees of smoothness of the surface.

### C. Sensitivity to Size and Shape

The sensitivity of the CRM model to size and shape variations was further analyzed on the SW and BF subsets.

*1) Sidewall aneurysms:* In this subgroup (58 aneurysms, 23 ruptured), the performance of the unnormalized entropy $CR_h$ was compared to the best size and shape performers from Table II, namely $D_{max}$ and NSI.

First, rupture prediction was applied to the aneurysms set using their $D_{max}$ as the only classification feature. This analysis labeled correctly 12 out of the 23 ruptured aneurysms (52%). Mean $D_{max}$ value of these 12 aneurysms was $9.47 \pm 0.68$mm.

Second, rupture prediction was applied to the aneurysms set using NSI as the only classification feature. This analysis labeled correctly 13 out of the 23 ruptured aneurysms (56%). Mean NSI value of these 13 aneurysms was $0.33 \pm 0.009$.

Third, rupture prediction was applied to the aneurysms set using the unnormalized entropy $CR_h$. This analysis labeled correctly 17 out of the 23 ruptured aneurysms (73%). All aneurysms correctly classified by either $D_{max}$ or NSI, were also correctly classified by $CR_h$. When looking at those aneurysms that were correctly classified by the CRM analysis, but mis-classified by the a$D_{max}$, our statistics show that these are smaller aneurysms (mean value $6.53 \pm 1.35$mm) with large non-sphericity indexes (mean value $0.33 \pm 0.05$). Similarly, when looking at those aneurysms that were correctly classified by the CRM analysis, but mis-classified by

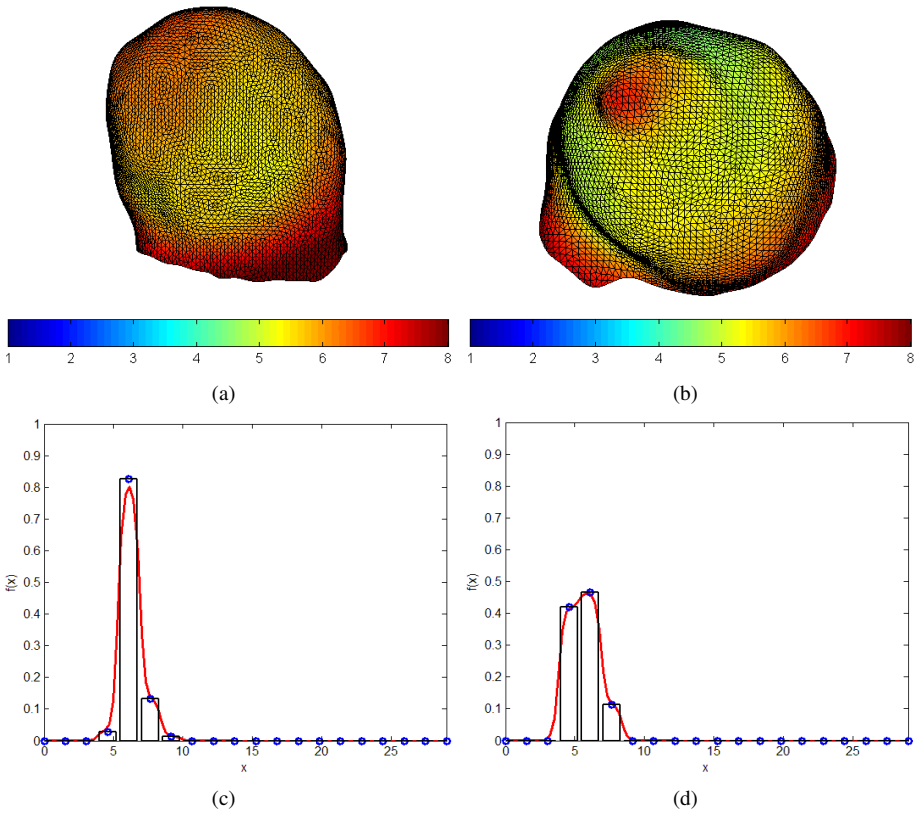


Fig. 5. Analysis results based on the *unnormalized* centroid-radii model on ruptured and unruptured SIDEWALL aneurysms. (a)Unruptured aneurysm. (b). Ruptured aneurysm (c) Histogram of the unruptured aneurysm.(d) Histogram of the ruptured aneurysm.

the NSI, our statistics show that these are large aneurysms (mean value $10.57 \pm 1.44$mm) with smaller NSI values (mean value $0.21 \pm 0.07$). These results reinforce the idea that the unnormalized entropy or CRM acts as an aggregate feature, which captures characteristics of both size and shape.

Note that although $D_{max}$ and NSI have good overall accuracy in the SW group (Table II), their accuracy in recognizing ruptured aneurysms is not impressive ($\approx 50\%$), which suggests good specificity, but poor sensitivity. In contrast, $CR_h$ shows higher accuracy both in the SW group, but also within the ruptured SW subset, suggesting high specificity and sensitivity.

*2) Bifurcation aneurysms:* In this subgroup (96 aneurysms, 50 ruptured), the performance of the normalized entropy of CRM was compared to the best size and shape performers from Table II, namely H/W and UI.

First, rupture prediction was applied to the aneurysms set using H/W as the only classification feature. This analysis labeled correctly 35 out of the 50 ruptured aneurysms (70%). Mean H/W of these 35 aneurysms was $1.64 \pm 0.38$mm.

Second, rupture prediction was applied to the aneurysms set using UI as the only classification feature. This analysis labeled correctly 34 out of the 50 ruptured aneurysms (68%). Mean UI value of these 34 aneurysms was $0.13 \pm 0.09$.

Third, rupture prediction was applied to the aneurysms set using the normalized entropy $CR_{hnorm}$. This analysis labeled correctly 39 out of the 50 ruptured aneurysms (78%). All aneurysms correctly classified by UI were also correctly classified by $CR_{hnorm}$. Two of the aneurysms correctly classified by H/W were misclassified by $CR_{hnorm}$. These are aneurysms with small neck and large height values, but with an otherwise smooth, regular shape. $CR_{hnorm}$ correctly classified as ruptured one additional aneurysm, which was misclassified by both H/W and UI. The aneurysm UI value was very close, but fell below the UI detection threshold.

Note that both H/W and UI have similar accuracy in the BF group (Table II) and within the ruptured BF subset. This suggests a good trade-off between their sensitivity and specificity. In contrast, $CR_{hnorm}$ shows good accuracy both in the BF group (70%), with even higher accuracy within the ruptured BF subset (78%), suggesting high specificity and sensitivity.

## VI. Discussions

This study introduces the entropies of the normalized and unnormalized centroid-radii model as novel 3D indexes, which are shown to be powerful discriminators of rupture status in intracranial aneurysms. The use of entropy allows for the extraction of a single shape index from the CRM distance distribution, a shape descriptor previously used exclusively in multidimensional form (histogram, distance arrays). While shape analysis is often based on scale invariance, it is demonstrated in this work that some applications benefit greatly from the use of both normalized and unnormalized versions of the same index. To the best of our knowledge, this is the first study using statistics derived from the CRM for medical imaging

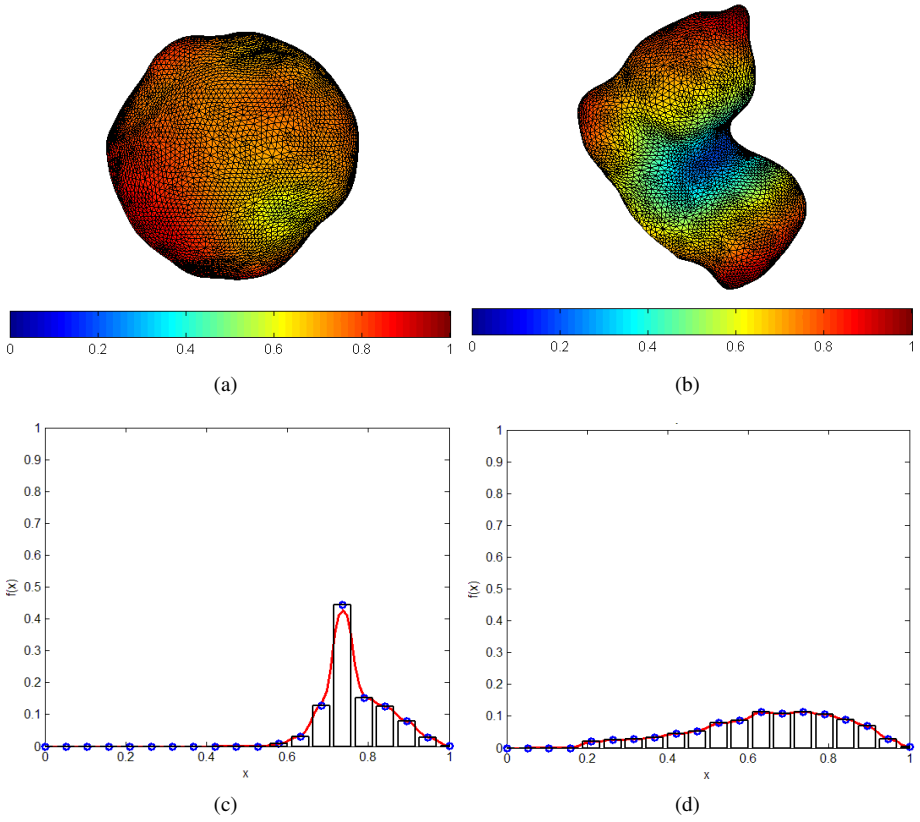


Fig. 6. Analysis results based on the *normalized* centroid-radii model on ruptured and unruptured BIFURCATION aneurysms. (a)Unruptured aneurysm. (b). Ruptured aneurysm (c) Histogram of the unruptured aneurysm (d) Histogram of the ruptured aneurysm.

applications. The centroid-radii model is intuitive, easy to use and its computation is completely automated.

In this work, SW and BF aneurysms are studied both as a compact group, but also as two separate subgroups. Recent research [29] and observations in our lab suggest a morphological split between the two subtypes, which is supported by the results from Tables II and III. On our dataset, the entropy of the CRM has a good performance for rupture status discrimination in both subtypes, when compared to six commonly used size and shape indexes. For SW aneurysms, using the entropy of the unnormalized distances resulted in rupture status prediction accuracy of 80.3% compared to 77.1% when using other established indexes. For BF aneurysms, using the entropy of the normalized distance distribution resulted in rupture status prediction accuracy of 70.5% compared to 66.8% when using other established size and shape indexes.

The use of normalized vs. unnormalized distances indicates that both size and shape influence rupture status in SW aneurysms, whereas mostly shape influences rupture status in BF aneurysms. This result is also supported by the classification analysis detailed in Table II. Indeed, our results indicate that rupture status discrimination is more challenging on BF aneurysms and all indexes presented here performed better on SW compared to BF aneurysms. It is however encouraging that the best performers in the BF group ($CR_{hnorm}$, H/W and UI) tend to have good sensitivity (good rupture recognition) compared to the best performers in the SW group (Sec. V-C). More research is needed to further analyze the split suggested here and to determine if indeed there are inherent morphological and possible hemodynamic differences between the two subtypes. Such an approach could lead to a better understanding of BF aneurysms and to better indexes for rupture status discrimination within this subgroup.

Our results show that misclassified BF aneurysms tend to be small aneurysms with a smooth, more regular shape. There is increasing evidence [13], [30], [31] that in addition to aneurysm sac morphology, the relationship between the aneurysm and its parent vessels is related to aneurysm rupture status. This relationship (inflow angle, parent vessel size, aneurysm inclination) may prove to be especially important for BF aneurysms, and we plan to explore this possibility in future work.

Robustness analysis shows the classification based on the centroid-radii model is insensitive to the segmentation method. This is an important and encouraging finding which suggests that a general classification function could be defined and potential users do not need to build their own training sets in order to use the index for rupture status prediction.

The fact that aneurysms are mostly star-shaped with respect to their centroids suggests that the centroid-radii computation can be further simplified for this particular application and the distances between the centroid and the aneurysm surface can be considered directly without checking for surface intersections. This would simplify the implementation and improve computation times (currently 128 seconds on average per study on an Intel dual-core T7600 (2.33GHz), 2GB RAM ). This

assumption will be further analyzed in future studies.

Similar to previous morphological research, the current study premise is based on an yet unproven assumption that aneurysms do not change shape and size upon rupture [9]–[11], [13]. This is still a point of contention and there is not enough information to decidedly settle the debate. Some studies report no major change in size and shape after rupture [18], [32], whereas the ISUIA study [6] contends that ruptured aneurysms data should not be used to draw conclusions about unruptured aneurysms evolution.

As in other retrospective studies [9]–[11], [13], the current analysis is performed on a dataset of aneurysms which were labeled as being ruptured or not at the time of detection. The evolution of these aneurysms was not followed clinically over time. As such we differentiate between predicting aneurysms rupture status and predicting rupture likelihood. Prospective studies, where in-vivo aneurysms are followed over long periods of time until they rupture or not, would determine if the usefulness of the centroid-radii model can be extended from predicting rupture status to determining rupture likelihood.

While the analysis was performed on a relatively large database and the results are encouraging, the eventual added value of the method remains to be determined in the clinical setting and, as mentioned above, would require validation in prospective clinical trials.

ELECTRONIC MATERIAL: This paper has supplementary downloadable material available at http://ieeexplore.ieee.org, provided by the authors. This includes performance comparison of four classifiers and additional illustrative results of ruptured and unruptured aneurysms.

## REFERENCES


[1] G. J. Rinkel, M. Djibuti, A. Algra, and J. van Gijn, "Prevalence and risk of rupture of intracranial aneurysms: a systematic review," *Stroke*, vol. 29, no. 1, pp. 251–256, 1998.

[2] J. M. Wardlaw and P. M. White, "The detection and management of unruptured intracranial aneurysms." *Brain*, vol. 123, no. 2, pp. 205–221, 2000.

[3] S. Q. Wolfe, M. K. Baskaya, R. C. Heros, and R. P. Tummala, "Cerebral aneurysms: learning from the past and looking toward the future," *Clin. Neurosurg.*, vol. 53, p. 157178, 2006.

[4] D. O. Wiebers, "Patients with small, asymptomatic, unruptured intracranial aneurysms and no history of subarachnoid hemorrhage should generally be treated conservatively: for." *Stroke*, vol. 36, pp. 408–409, 2005.

[5] B. Weir, "Patients with small, asymptomatic, unruptured intracranial aneurysms and no history of subarachnoid hemorrhage should generally be treated conservatively: against." *Stroke*, vol. 36, pp. 4010–411, 2005.

[6] D. O. Wiebers, "Unruptured intracranial aneurysms: natural history, clinical outcome, and risks of surgical and endovascular treatment," *The Lancet*, vol. 362, no. 9378, pp. 103 – 110, 2003.

[7] T. I. S. of Unruptured Intracranial Aneurysm Investigators, "Unruptured intracranial aneurysmsrisk of rupture and risk of surgical intervention," *N Engl J Med*, vol. 339, p. 17251733, 1998.

[8] B. L. Hoh, C. L. Sistrom, C. S. Firment, G. L. Fautheree, G. J. Velat, J. H. Whiting, J. F. Reavey-Cantwell, and S. B. Lewis, "Bottleneck factor and height-width ratio: Association with ruptured aneurysms in patients with multiple cerebral aneurysms," *Neurosurgery*, vol. 61, no. 4, pp. 716–723, 2007.

[9] M. L. Raghavan, B. Ma, and R. E. Harbaugh, "Quantified aneurysm shape and rupture risk," *Journal of neurosurgery*, vol. 102, no. 2, pp. 355–362, 2005.

[10] S. Dhar, M. Tremmel, J. Mocco, M. Kim, J. Yamamoto, A. H. Siddiqui, L. N. Hopkins, and H. Meng, "Morphology parameters for intracranial aneurysm rupture risk assessment," *Neurosurgery*, vol. 63, no. 2, pp. 185–197, 2008.

[11] B. S. Ma, R. E. Harbaugh, and M. L. Raghavan, "Three-dimensional geometrical characterization of cerebral aneurysms," *Annals of Biomedical Engineering*, vol. 32, no. 2, pp. 264–273, FEB 2004.

[12] S. Rohde, K. Lahmann, J. Beck, R. Nafe, B. Yan, A. Raabe, and J. Berkefeld, "Fourier analysis of intracranial aneurysms: towards an objective and quantitative evaluation of the shape of aneurysms," *Neuroradiology*, vol. 47, no. 2, pp. 121–126, 2005.

[13] R. D. Millan, L. Dempere-Marco, J. M. Pozo, J. R. Cebral, and A. F. Frangi, "Morphological characterization of intracranial aneurysms using 3-d moment invariants," *IEEE Transactions on Medical Imaging*, vol. 26, no. 9, pp. 1270–1282, SEP 2007.

[14] C. C. Chang, S. M. Hwang, and D. J. Buehrer, "A shape recognition scheme based on relative distances of feature points from the centroid," *Pattern Recognition*, vol. 24, no. 11, pp. 1053–1063, 1991.

[15] K.-L. Tan, B. C. Ooi, and L. F. Thiang, "Indexing shapes in image databases using the centroid-radii model," *Data & Knowledge Engineering*, vol. 32, pp. 271–289, 2000.

[16] ——, "Retrieving similar shapes effectively and efficiently," *Multimedia Tools and Applications*, vol. 19, pp. 111–134, 2003.

[17] X. Kong, Q. Luo, G. Zeng, and M. H. Lee, "A new shape descriptor based on centroid-radii model and wavelet transform," *Optics Communications*, vol. 273, no. 2, pp. 362 – 366, 2007.

[18] H. Ujiie, H. Tachibana, O. Hiramatsu, A. L. Hazel, T. Matsumoto, Y. Ogasawara, H. Nakajima, T. Hori, K. Takakura, and F. Kajiya, "Effects of size and shape (aspect ratio) on the hemodynamics of saccular aneurysms: A possible index for surgical treatment of intracranial aneurysms," *Neurosurgery*, vol. 45, no. 1, pp. 119–130, 1999.

[19] D. Vranic and D. Saupe, "3d medel retrieval," in *Spring Conference on Computer Graphics and its Applications*. Comenius University Slovakia, 2000, pp. 89–93.

[20] D. Saupe and D. Vranic, "3d model retrieval with spherical harmonics and moments," in *Proceedings of DAGM*. Munich, 2001, pp. 392–397.

[21] B. A. Coert, S. D. Chang, H. M. Do, M. P. Marks, and G. K. Steinberg, "Surgical and endovascular management of symptomatic posterior circulation fusiform aneurysms," *J Neurosurg*, vol. 106, p. 855865, 2007.

[22] J. O. Bescos, M. J. Slob, C. H. Slump, M. Sluzewski, and W. J. van Rooij, "Volume measurement of intracranial aneurysms from 3d rotational angiography: Improvement of accuracy by gradient edge detection," *AJNR Am J Neuroradiol*, vol. 26, no. 10, pp. 2569–2572, 2005. [Online]. Available: http://www.ajnr.org/cgi/content/abstract/26/10/2569

[23] C. D. Hansen and C. R. Johnson, *The visualization handbook*. Elsevier Academic Press, 2004.

[24] W. Hardle, *Applied Nonparametric Regression*. Cambridge University Press, 1990.

[25] A. W. Bowman and A. Azzalini, *Applied Smoothing Techniques for Data Analysis*. Oxford University Press, USA, 1997.

[26] T. M. Cover and J. A. Thomas, *Elements of information theory*, 2nd ed. Wiley, 2006.

[27] F. E. Harrell, "Regression modelling strategies for improved prognostic prediction," *Statistics in Medicine*, vol. 3, pp. 143–152, 1984.

[28] J. A. Sethian, *Level set methods and fast marching methods*. Cambridge University Press, 1999.

[29] M. I. Baharoglu, C. M. Schirmer, D. A. Hoit, B.-L. Gao, and A. M. Malek, "Aneurysm Inflow-Angle as a Discriminant for Rupture in Sidewall Cerebral Aneurysms: Morphometric and Computational Fluid Dynamic Analysis," *Stroke*, vol. 41, no. 7, pp. 1423–1430, 2010.

[30] A. Lauric, E. Miller, M. I. Baharoglu, and A. M. Malek, " 3D shape analysis of intracranial aneursyms using the writhe number as a discriminant for rupture." *Annals of Biomedical Engineering*, 2011.

[31] J. Xiang, S. K. Natarajan, M. Tremmel, D. Ma, J. Mocco, L. N. Hopkins, A. H. Siddiqui, E. I. Levy, and H. Meng, "Hemodynamic-morphologic discriminants for intracranial aneurysm rupture," *Stroke*, vol. 42, no. 1, pp. 144–152, 2011. [Online]. Available: http://stroke.ahajournals.org/cgi/content/abstract/42/1/144

[32] M. Rahman, C. S. Ogilvy, G. J. Zipfel, C. P. Derdeyn, A. H. Siddiqui, K. R. Bulsara, L. J. Kim, H. A. Riina, J. Mocco, and B. L. Hoh, "Unruptured cerebral aneurysms do not shrink when they rupture: multicenter collaborative aneurysm study group," *Neurosurgery*, vol. 68, no. 1, pp. 155–60; discussion 160–1, 2011.